Supplementary Information for:

Geodynamic implications of synchronous norite and TTG formation in the 3 Ga Maniitsoq Norite Belt, West Greenland

Pedro Waterton, William R. Hyde, Jonas Tusch, Julie A. Hollis, Christopher L. Kirkland, Carson Kinney, Chris Yakymchuk, Nicholas J. Gardiner, David Zakharov, Hugo Olierook, Peter C. Lightfoot, Kristoffer Szilas

A1 Additional examples of granoblastic textures

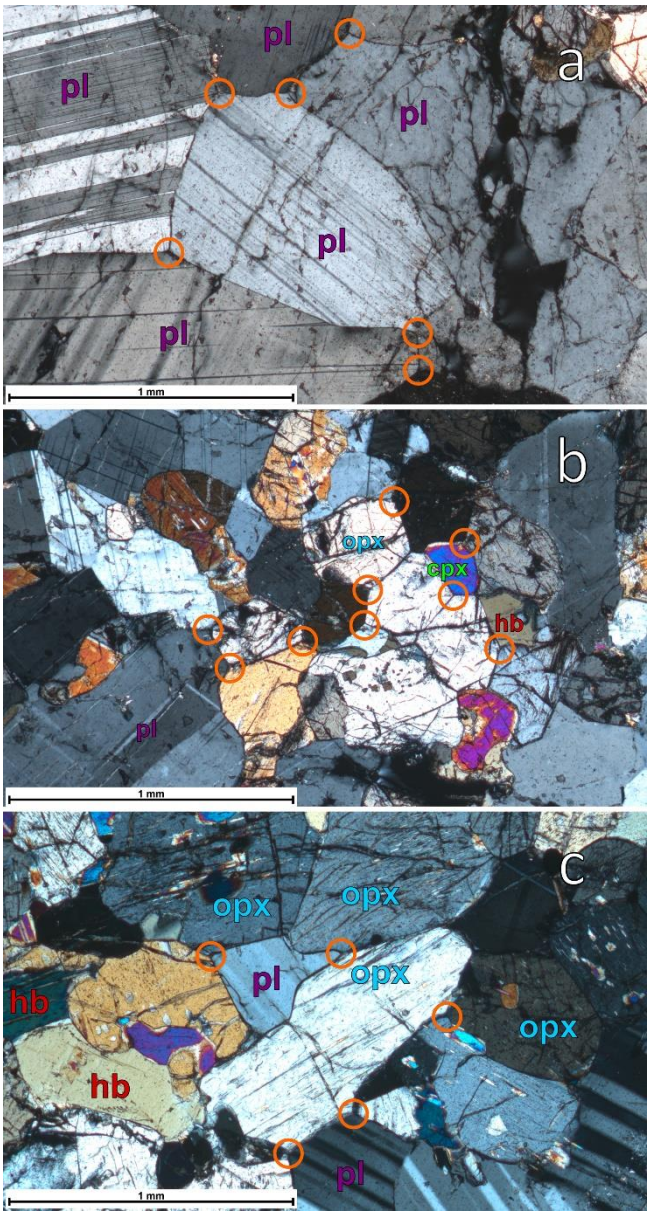

Figure A1: Cross-polarised light photomicrographs showing examples of granoblastic textures in two norite samples (a, b) and one melanorite (c). Orange circles highlight well-equilibrated grain boundary triple junctions. Orthopyroxene (opx), clinopyroxene (cpx), plagioclase (pl) and hornblende (hb) are identified.

A2 Analytical methods

A2.1 EPMA mineral chemistry

Chemical compositions of major mineral phases in norite belt samples were determined using a JEOL JXA-8200 Superprobe at the University of Copenhagen, in wavelength dispersive mode. Typical mineral analyses used an accelerating voltage of 15 kV, beam current of 15 nA, 20 s count times on both peak and backgrounds, and a spot size of 5 µm. Matrix corrections were performed using a ϕ(ρz) correction.

A2.2 Bulk-rock major and trace elements

Bulk-rock major and trace element compositions were determined for all samples at ALS Laboratories (Ireland). Samples were crushed, split using a riffle splitter, and powdered in a low Cr steel mill. Major element concentrations were obtained using the ME-ICP06 analytical package, in which samples are dissolved by Li-metaborate fusion and analysed by ICP-AES. Trace element concentrations were determined by ICP-MS in separate powder splits, with one part dissolved by Li-metaborate fusion (ME-MS81 package) and the other by four-acid digestion (ME-MS61 package). Due to concerns over data quality, including quantisation of low concentration trace element data and large degrees of scatter in conservative elements such as the HREEs, a subset of 42 samples were reanalysed for major and trace element compositions at Peter Hooper Geoanalytical Lab at Washington State University (WSU). Samples were crushed using a steel hydraulic press and steel jaw crusher, split using a rotary splitter, and finely powdered in an agate ball mill. Major elements, and some trace elements, were analysed by XRF on Li-tetraborate beads (Johnson *et al.*, 1999). Trace elements were analysed on an Agilent model 4500 ICP-MS following a two-step di-Lithium tetraborate fusion followed by mixed acid digestion method. Repeatability of the trace element analyses is typically better than 10% (2σ relative) for the REEs and better than 20% for all other trace elements (Knaack *et al.*, 1994; Waterton *et al.*, 2020). Replicate analyses of two samples show good agreement, and elements analysed by both XRF and ICP-MS are in good agreement (supplementary table 1).

A comparison of the ALS and WSU data showed that the major element data and a few select minor and trace elements (Ni, Cr, Sc, V, Sr, Cu) from ALS labs were of sufficient quality for further use. However, the remaining trace elements are not considered accurate and/or precise and are not used further in this study. The ALS data is therefore largely used to broaden the range of major element data in this study and all discussions of trace element data concern the samples reanalysed at WSU.

A2.3 Platinum group element (PGE) analyses

Platinum group elements were analysed for 19 samples at Laboratoire des Matériaux Terrestres, Université du Québec à Chicoutimi, using 15 g of bulk-rock powder for each sample prepared at ALS Labs. Ten norite

samples were selected, all from the largest norite body (Fossilik), and nine melanorite samples were selected from a number of smaller bodies in the norite belt. The PGEs were isolated using nickel-sulphur fire assay (NiS-FA), followed by $SnCl_2.2H_2O$–Te co-precipitation (Savard *et al.*, 2010). The precipitate was dissolved in a 1:1 HCl and HNO_3 mixture, then diluted for ICP-MS analysis on a Thermo Elemental X7 series, with concentrations determined by external calibration using a mixed PGE-Au stock solution. Accuracy of the analyses were monitored through an analysis of the OKUM komatiite reference material along with the samples, which shows good agreement with previously published values (supplementary table 1). Repeatability of the analyses, estimated from repeated analyses of the OKUM standard, is expected to be < 25% ($2\sigma_{rel}$) for all elements except Os, Re and Au (Savard *et al.*, 2010), which are not reported here due to their poor analytical precision.

A2.4 ^{147}Sm-^{143}Nd and ^{176}Lu-^{176}Hf sample digestion and purification

^{147}Sm-^{143}Nd and ^{176}Lu-^{176}Hf isotopic analyses were carried out at the Institut für Geologie und Mineralogie, Universität zu Köln, using the sample powders prepared at ALS Labs, and the same subset of samples analysed for PGEs. Approximately 120 mg of each sample was precisely weighed and mixed with appropriate amounts of isotopically enriched ^{176}Lu–^{180}Hf and ^{149}Sm–^{150}Nd spikes. The samples were then digested using a two-step dissolution procedure modified from Hoffmann et al. (2011) to ensure complete dissolution of resistant Hf-bearing phases, such as zircon. First, samples were digested at 130 °C for 24 hours in a 1:1 mixture of concentrated HF:HNO_3 on an open hotplate. The samples were dried down before a second stage 180 °C, 48 hour dissolution in a 3:1 mixture of concentrated HF:HNO_3 in Parr® bombs. The HF:HNO_3 mixture was evaporated to near-dryness, and the samples were evaporated to near-dryness in concentrated HNO_3 three times to prevent the formation of insoluble fluorides. Finally, the samples were dried and digested in 6 N HCl–0.06 HF to complete spike-sample equilibration. Lu and Hf were separated using Eichrom® Ln-spec resin (Münker *et al.*, 2001; Weyer *et al.*, 2002). LREEs were separated from the remaining matrix using standard cation exchange techniques (AG 50W X8 resin), before separation of Sm and Nd using Eichrom® Ln-spec resin (Pin and Zalduegui, 1997).

Lutetium, Hf, Sm and Nd were measured on a Thermo Scientific Neptune multi-collector ICP-MS (MC-ICP-MS). Measured $^{176}Hf/^{177}Hf$ were mass bias corrected to $^{179}Hf/^{177}Hf = 0.7325$ (Patchett and Tatsumoto, 1981) using an exponential law. Data are given relative to $^{176}Hf/^{177}Hf = 0.282160$ for the AMES Hf solution, isotopically indistinguishable from the JMC-475 standard (Scherer *et al.*, 2000), which was analysed interspersed with the samples at a similar Hf concentration. Measured $^{143}Nd/^{144}Nd$ data were mass bias corrected to $^{146}Nd/^{144}Nd = 0.7219$ for using an exponential law. Data are given relative to $^{143}Nd/^{144}Nd = 0.512115$ for JNdi (i.e., 0.511858 for the LaJolla Nd standard solution; Tanaka et al., 2000), based on analyses of the AMES, JNdi, and LaJolla Nd solution interspersed with the samples at a similar Nd

concentration. Data was blank corrected based on the average of three total procedural blanks analysed with the samples: Lu = 3.7 pg, Nd = 50 pg, Sm = 50 pg, except for Hf, which was corrected using the long term average blank of 781 pg due to its greater variability (average of three blanks measured for this study = 1267 pg). Precision and accuracy of the analyses were monitored through two analyses of BHVO-2, which show good agreement to reference values (supplementary table 1; Jochum et al., 2005).

A2.5 Oxygen isotope analyses

Six bulk rock norite samples and two plagioclase separates from the Fossilik body were analysed for oxygen isotopes ($\delta^{18}O$) at the University of Oregon Stable Isotope Laboratory. Between 1.5 and 2.5 mg of bulk rock samples and mineral separates were placed in a stainless steel chamber connected to the laser fluorination line composed of 1/4" stainless steel tubing held under vacuum. Oxygen gas was liberated by heating the samples with an infrared laser (35W New Wave Research) in presence of BrF_5 reagent. Extracted oxygen was purified through a series of cryogenic traps immersed in liquid nitrogen and further passed through Hg-diffusion pump to remove traces of fluorine-containing gases. The resulting O_2 gas was converted to CO_2 gas in a heated platinum-graphite converter. After the yields were measured, the CO_2 gas was measured for $\delta^{18}O$ in a MAT 253 mass spectrometer in dual inlet mode. To monitor the accuracy of analyses several aliquots of an internal standard (UOG garnet with $\delta^{18}O$ = 6.52 ‰) were analysed within each analytical session. The deviations from the nominal value of the standard (not exceeding 0.3 ‰) were used to correct the values of unknowns.

A2.6 U-Pb zircon geochronology

U-Pb measurements were performed using in-situ analytical techniques on zircon separates from four norite belt samples and an intrusive TTG sheet. Zircon grains were separated from each sample using magnetic and heavy liquid techniques. The zircon grains, together with zircon reference standards, were cast in epoxy mounts, which were then polished to approximately a half-grain thickness for analysis. Each mount was documented with transmitted and reflected light micrograph images, and cathodoluminescence (CL) imaging was performed to provide information on internal textures to aid further interpretation, prior to analysis. U-Pb geochronology was performed at the John de Laeter Centre Curtin University, using either LA-ICP-MS or a SHRIMP II ion microprobe.

All LA-ICP-MS analytical sessions used a RESOlution 193 nm excimer laser set to a ~30 µm spot size, an on-sample fluence of 2.8 J cm^{-2} and repetition rate of 10 Hz for ~25 s of total analysis time and 35 s of background capture. All analyses were preceded by two cleaning pulses. The sample cell was flushed by ultrahigh purity He (0.35 L min^{-1}) and N_2 (1.2 mL min^{-1}). LA-ICP-MS analyses were made using an Agilent 7700s single quadrupole or an Agilent 8900 triple quadrupole ICP-MS mass spectrometer (see

supplementary table 4), with high purity Ar as the carrier gas for both sessions (flow rate 0.98 L min^{-1}). Analyses of every 10 unknowns were bracketed by analysing a standard block containing the primary zircon reference materials OG1 (3465.4 Ma ± 0.6 Ma; $^{207}Pb/^{206}Pb$ age; Stern *et al.*, 2009) and, for the triple quadrupole only, 91500 (1062.4 ± 0.4 Ma; $^{206}Pb/^{238}U$ age; Wiedenbeck *et al.*, 1995; Horstwood *et al.*, 2016). OG1 was used as the principal age standard as it has a similar ablation response to the unknowns investigated in this work, with 91500 used on the triple quadrupole to validate $^{206}Pb/^{238}U$ ratios (with secondary reference materials) and U and Th concentrations. Secondary reference zircons GJ-1 (601.9 ± 0.4 Ma; $^{206}Pb/^{238}U$ age; Jackson *et al.*, 2004; Horstwood *et al.*, 2016), Plešovice (337.13 ± 0.37 Ma; $^{206}Pb/^{238}U$ age; Sláma et al., 2008), and Maniitsoq (triple quadrupole only; 3008.70 ± 0.72 Ma; $^{207}Pb/^{206}Pb$ age; Marsh *et al.*, 2019) were also used to monitor data accuracy and precision. In the analytical sessions, all secondary standards yielded weighted mean ages within 2σ of the published ages ($p > 0.05$; see full standard data in supplementary table 4). $^{206}Pb/^{238}U$ ages calculated for all zircon age standards, treated as unknowns, are found to be within 1% of the accepted value when matrix matched standards are used in the data reduction. All ages are reported with ± 2σ uncertainties calculated directly from isotopic ratios. Age data are filtered for concordance, and ages outside a ± 10% discordance threshold are regarded as discordant. The time-resolved mass spectra were reduced using the U-Pb geochronology data reduction schemes in Iolite3™ (Paton *et al.*, 2011), and in-house Microsoft Excel macros. No common lead corrections were deemed necessary due to generally low ^{204}Pb counts. Those analyses with elevated ^{204}Pb counts are not used in placing age constraints.

For the ion microprobe analyses, U–Th–Pb ratios and absolute abundances were determined relative to the CUYZ standard zircon ($^{206}Pb/^{238}U$ age = 568.55 Ma; $^{207}Pb/^{206}Pb$ age = 569.49 Ma; U = 582.7 ppm; Th = 82.7 ppm; Mole *et al.*, 2018; Tedeschi *et al.*, 2020; A. Kennedy, pers. comms.), analyses of which were interspersed with those of unknown zircons and secondary reference material Plešovice (337.13 ± 0.37 Ma; Sláma et al., 2008). Fractionation of $^{206}Pb^*/^{238}U$ (Pb* = radiogenic Pb) was monitored during each session and no fractionation correction was deemed necessary. Plešovice yielded a $^{206}Pb^*/^{238}U$ weighted mean age of 337.7 ± 3.0 (MSWD = 0.52), which overlaps the published age within uncertainty. Measured compositions were corrected for common Pb using measured ^{204}Pb. Prior to analysis, each site was cleaned by rastering the primary ion beam over the area for up to 2.5 minutes. In most cases, corrections are sufficiently small to be insensitive to the choice of common Pb composition, and an average crustal composition (Stacey and Kramers, 1975) appropriate to the age of the mineral was assumed, as generally common Pb counts did not fall during the analyses (i.e., common Pb is not surface derived). Data were reduced using SQUID, in-house macros, and Isoplot (Ludwig, 2009, 2012), using decay constants of Steiger and Jäger (1977).

Full U-Pb isotopic data for the samples and reference materials are given in supplementary table 4. Data are reported following the guidelines of the Geological Society of London (2015), with derivative ratios

recommended by Horstwood *et al.* (2016) also included. Both internal and external sources of uncertainty were propagated in quadrature, inflation for a coherent secondary reference material was not required for any of the sessions in this study as all secondary standards overlapped published values within uncertainty. Calculated mean ages are quoted in the text with 95% uncertainties (tσ√MSWD; Ludwig, 2012) and the value of the mean square of weighted deviates (MSWD). Total systematic uncertainties in $^{207}Pb/^{206}Pb$ ages = 0.14% (2σ relative), corresponding to an uncertainty of approximately 4 Myrs. However, these uncertainties are dominated by uncertainties in the $^{238}U/^{235}U$ ratio and decay constants, with only a small contribution (~0.02% 2σ relative) from uncertainties in the primary reference material accepted values. These systematic uncertainties therefore have a minimal effect on inter-lab comparisons of zircon ages (Section 6.1) calculated using the same $^{238}U/^{235}U$ ratio and decay constants, and were not propagated into the mean ages.

A2.7 Phase equilibrium modelling

Phase equilibrium modelling was used to determine the predicted mineral assemblages as a function of P–T conditions for one norite sample (1045) and one melanorite sample (1427), chosen as representative compositions for each group. Phase assemblages were modelled in the NCKFMASHTOCr (Na_2O–CaO–K_2O–FeO–MgO–Al_2O_3–SiO_2–H_2O–TiO_2–O–Cr_2O_3) chemical system using the Holland and Powell (2011) database (ds63 update) and the activity–composition models of Holland et al. (2018) for liquid, clinopyroxene, orthopyroxene, olivine, garnet, and spinel; Holland and Powell (2003) for plagioclase; White et al. (2000) for ilmenite; White et al. (2014) for biotite; and, Green et al. (2016) for clinoamphibole (e.g., hornblende). Quartz, sphene, rutile and H_2O were treated as pure end-members. Calculations were conducted using the THERMOCALC (v.3.47) software package (Powell and Holland, 1988). Mineral abbreviations are from Holland and Powell (2011). Modelling results are sensitive to the relative amounts of ferric and ferrous iron, and each modelled composition was assumed to have 10 mol% of the total iron as Fe^{3+}. Both samples were modelled assuming H_2O equal to the loss-on-ignition value (LOI). Sample 1045 was also modelled under water-saturated conditions to investigate possible retrogressive mineral assemblages as a function of P-T. Modelled compositions are given in supplementary table 2.

A3 Supplementary Results

A3.1 Pyroxene chemistry and thermobarometry

Pyroxene compositions in the norites and melanorites strongly correlate with bulk rock composition (Figure A2), which we interpret to indicate equilibration of the pyroxenes with bulk rock compositions during metamorphism. There is a consistent offset of ~0.1 Mg# units between orthopyroxene and clinopyroxene in the same sample.

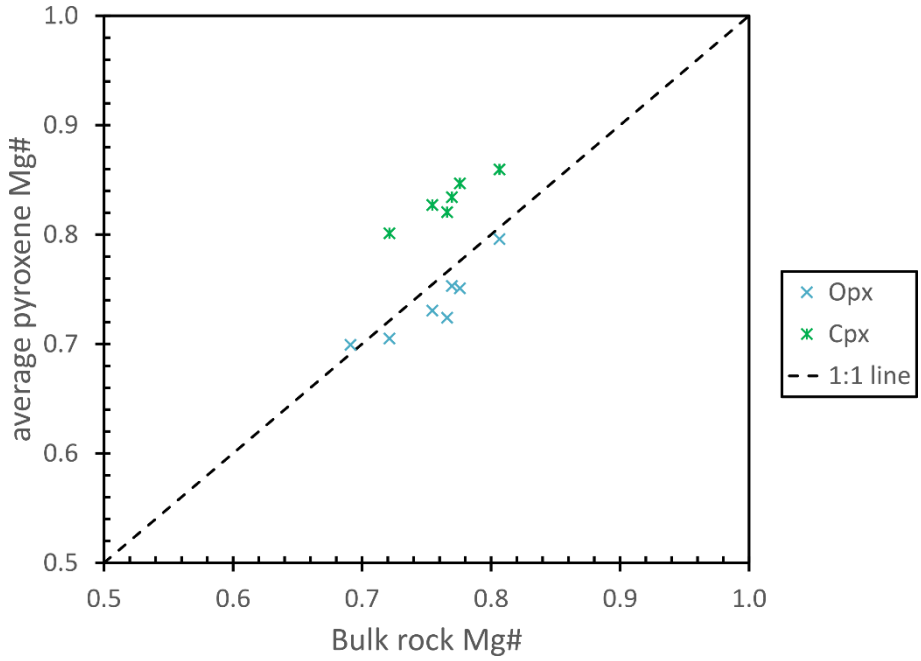

Figure A2: Plot of average orthopyroxene and clinopyroxene compositions against bulk rock Mg# for norite and melanorite samples.

Pyroxene equilibration temperatures are estimated using the graphical two-pyroxene thermometer of Lindsley and Andersen (1983). Temperatures estimated for individual analyses show significant scatter, potentially due to uncertainties introduced through calculation of tetrahedral Al based on Si, calculation of Fe^{3+} based on charge balance, and the presence of fine lamellae and inclusions of amphibole within the pyroxenes. To reduce the influence of these uncertainties, we calculate equilibration temperatures from average compositions of melanorite and norite ortho- and clinopyroxenes. Furthermore, we consider the temperatures from clinopyroxene compositions to be more reliable due to the extremely close spacing of temperature contours around the measured orthopyroxene compositions. Average norite cpx compositions plot at ~750 °C at 1 atm, corresponding to pressure-corrected temperatures of ~767 °C at 5 kb or 781 °C at 9 kb (the maximum pressure estimated from phase equilibrium modelling constraints). Average melanorite opx compositions plot on the 800 °C contour, corresponding to pressure-corrected temperatures of ~818 °C at 5 kb or 833 °C at 9 kb. The pyroxenes have low proportions of non-quadrilateral components (~2 mol%), suggesting uncertainties of ± 50 °C (Lindsley and Andersen, 1983). Considering the poorly constrained

minimum pressure of metamorphism, we conservatively assume an uncertainty of ± 70 °C, and interpret the pyroxene compositions to reflect equilibration temperatures of ~780 ± 70 °C in the norites, and ~830 ± 70 °C in the melanorites.

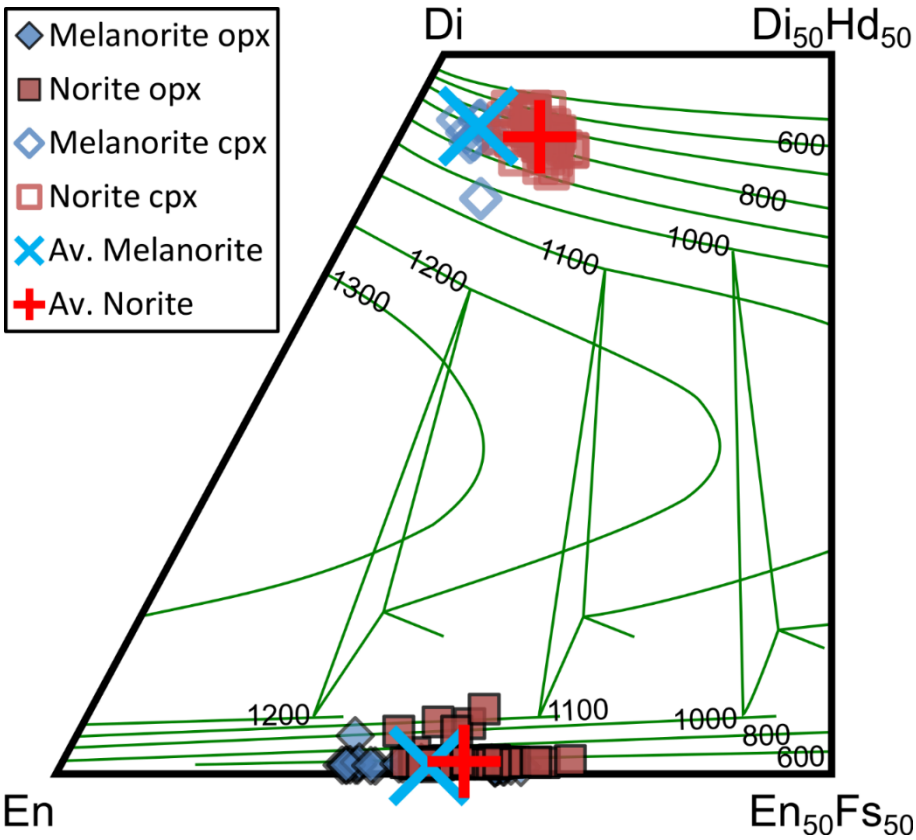

Figure A3: Pyroxene compositions plotted on the pyroxene quadrilateral following the projection scheme of Lindsley and Andersen (1983). Temperature contours (green lines, temperatures in °C) are atmospheric pressure contours from Lindsley and Andersen (1983). The average melanorite clinopyroxene composition lies on the 800 °C contour, average norite clinopyroxene composition lies between the 700 °C and 800 °C contours at ~750 °C. Average orthopyroxene compositions for both norites and melanorites lie between the 600 and 800 °C contours, but are poorly constrained due to the close spacing of contours in this part of the diagram.

A3.2 U-Pb zircon geochronology

A3.2.1 Sample 565 – melanorite

Sample 565 is a melanorite from a moderately sized norite body towards the southwest end of the belt. Zircon crystals from sample 565 are subhedral and range in length from 50 µm to 150 µm. Under CL, the grains display oscillatory zoning, with evidence for minor later rim growth. The zircons have generally low U contents (~65 ppm), moderate Th/U ratios (~1.3), and show consistent slight discordance in U-Pb space. The low U content leads to lower radiogenic-Pb count rates. All eight analyses of oscillatory-zoned zircon yield a weighted mean $^{207}Pb/^{206}Pb$ age of 3025 ± 12 Ma (MSWD 1.5), interpreted as the best estimate of the magmatic age of the rock.

A3.2.2 Sample 585 – melanorite

Sample 585 is a mineralised (pentlandite-bearing) melanorite recovered from drill core. The zircon crystals are euhedral with high length to width ratios of up to 6:1. In CL images, the grains display oscillatory zoning and frequently have a high CL response rim (low U). Two analyses are > 10% discordant and not considered further. Thirteen analyses of oscillatory zoned zircon yielded a weighted mean $^{207}Pb/^{206}Pb$ age of 3003 ± 9 Ma (MSWD = 1.0), interpreted as the age of magmatic crystallization.

A3.2.3 Sample 875 – melanorite

Sample 875 is a spotted norite from the northern part of the belt, located just east of the Fossilik norite body (Ravenelle *et al.*, 2017). The zircon crystals are euhedral to subhedral and have low to moderate length to width ratios of 1:1 to 4:1. Grains are relatively large, with widths >100 µm. Some grains show small, rounded, metamict xenocrystic cores, which were avoided during analysis. Rims are absent. One analysis is interpreted as a mixture of different domains and is not considered further. Twenty analyses were conducted on grains that show well-developed sector- and oscillatory-zoned cores. These have very low to moderate U concentrations (16–126 ppm), low to moderate Th/U ratios (0.36–3.09), and yielded a weighted mean $^{207}Pb/^{206}Pb$ age of 3010 ± 3 Ma (MSWD = 1.5), interpreted as the age of magmatic crystallization.

A3.2.4 Sample 811 – norite

Sample 811 is a coarse grained norite from Imiak Hill norite body (Ravenelle *et al.*, 2017), located towards the northern end of the norite belt. The zircon crystals are euhedral to anhedral and have low to moderate length to width ratios of 1:1 to 3:1. One analysis is interpreted as a mixture and is not considered further. Twenty-two analyses were conducted on grains that show faint sector or oscillatory zoning. These grains have moderate to high U concentrations (88–554 ppm) and moderate Th/U ratios (0.88–1.73), and yielded a weighted mean $^{207}Pb/^{206}Pb$ age of 3000 ± 4 Ma (MSWD = 0.40), interpreted as the magmatic crystallisation

age of the sample.

A3.2.5 Sample 1013 – TTG sheet intruding norite

Sample 1013 is from a TTG sheet intruding a norite body from near the centre of the norite belt, close to the boundary of the Finnefjeld Orthogneiss Complex. Melanorite sample 823, which has disturbed ^{147}Sm-^{143}Nd characteristics, was sampled adjacent to this sheet. The zircon crystals are euhedral to subhedral and have low to moderate length to width ratios of 1:1 to 4:1. Grains are relatively large with widths commonly more than 100 μm. Three analyses are > 5% discordant and are not considered further. Thirty-three analyses conducted on grains with oscillatory or sector zoning have low to moderate U concentrations (69–435 ppm) and low to moderate Th/U ratios (0.27–0.91). These 33 analyses yield a weighed mean $^{207}Pb/^{206}Pb$ age of 2989 ± 2 Ma (MSWD = 1.2), interpreted as the magmatic crystallisation age of the TTG sheet.

A4 Plots of trace elements against Yb – effect of metamorphism

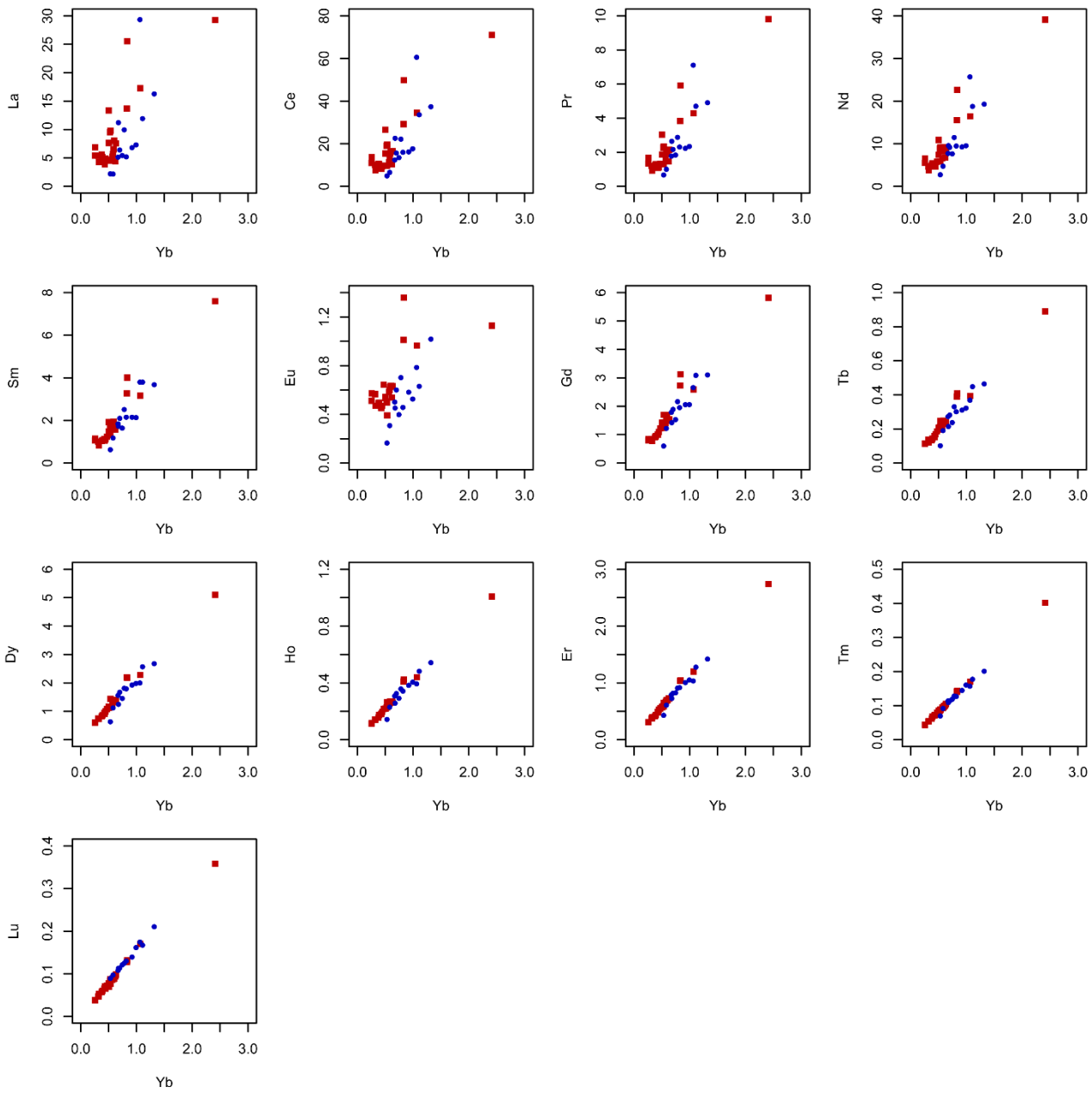

Figure A4: Plots of REEs against Yb, a conservative immobile element, to assess mobility of other REEs during metamorphism. Red squares = norites, blue circles = melanorites. See main text for discussion.

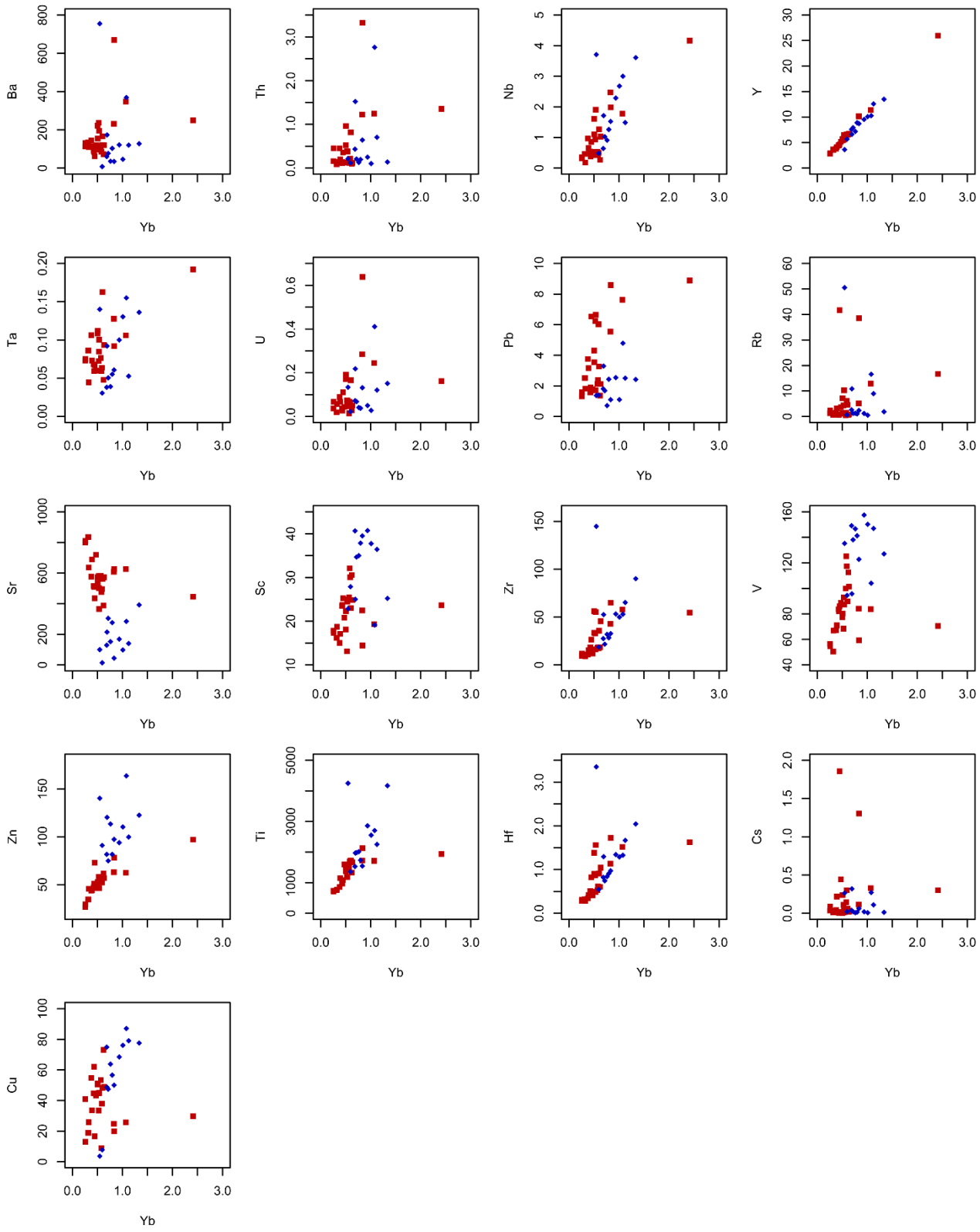

Figure A5: Plots of other incompatible trace elements against Yb, a conservative immobile element, to assess mobility of trace elements during metamorphism. Red squares = norites, blue circles = melanorites. See main text for discussion.

References

Geological Society of London reporting standards for 40 Ar- 39 Ar and U-Pb geochronometric data (2015).

Green, E. C. R., White, R. W., Diener, J. F. A., Powell, R., Holland, T. J. B. & Palin, R. M. (2016). Activity–composition relations for the calculation of partial melting equilibria in metabasic rocks. *Journal of Metamorphic Geology* **34**, 845–869.

Hoffmann, J. E., Münker, C., Næraa, T., Rosing, M. T., Herwartz, D., Garbe-Schönberg, D. & Svahnberg, H. (2011). Mechanisms of Archean crust formation inferred from high-precision HFSE systematics in TTGs. *Geochimica et Cosmochimica Acta* **75**, 4157–4178.

Holland, T. J. B., Green, E. C. R. & Powell, R. (2018). Melting of Peridotites through to Granites: A Simple Thermodynamic Model in the System KNCFMASHTOCr. *Journal of Petrology* **59**, 881–900.

Holland, T. J. B. & Powell, R. (2011). An improved and extended internally consistent thermodynamic dataset for phases of petrological interest, involving a new equation of state for solids. *Journal of Metamorphic Geology* **29**, 333–383.

Holland, T. & Powell, R. (2003). Activity–composition relations for phases in petrological calculations: an asymmetric multicomponent formulation. *Contributions to Mineralogy and Petrology* **145**, 492–501.

Horstwood, M. S. A. *et al.* (2016). Community-Derived Standards for LA-ICP-MS U-(Th-)Pb Geochronology – Uncertainty Propagation, Age Interpretation and Data Reporting. *Geostandards and Geoanalytical Research* **40**, 311–332.

Jackson, S. E., Pearson, N. J., Griffin, W. L. & Belousova, E. A. (2004). The application of laser ablation-inductively coupled plasma-mass spectrometry to in situ U-Pb zircon geochronology. *Chemical Geology* **211**, 47–69.

Jochum, K. P., Nohl, U., Herwig, K., Lammel, E., Stoll, B. & Hofmann, A. W. (2005). GeoReM: A New Geochemical Database for Reference Materials and Isotopic Standards. *Geostandards and Geoanalytical Research* **29**, 333–338.

Johnson, D. M., Hooper, P. R. & Conrey, R. M. (1999). XRF analysis of rocks and minerals for major and trace elements on a single low dilution Li-tetraborate fused bead. *Advances in X-ray Analysis* **41**, 843–867.

Knaack, C., Cornelius, S. & Hooper, P. (1994). Trace Element Analyses of Rocks and Minerals by ICP-MS. Open-file report, Department of Geology, Washington State University, Pullman.

Lindsley, D. H. & Andersen, D. J. (1983). A two-pyroxene thermometer. *Proceeedings of the thirteenth Lunar and Planetary Science Conference, Part 2. Journal of Geophysical Research* **88**, A887–A906.

Ludwig, K. (2009). SQUID 2: A user's manual, rev. 12. *Berkeley Geochronology Center Special Publications No. 5* 1–110.

Ludwig, K. R. (2012). User 's Manual for Isoplot, v3.75, A Geochronological Toolkit for Microsoft Excel. *Berkeley Geochronology Center Special Publications No. 5* 1–75.

Marsh, J. H., Jorgensen, T, R. C., Petrus, J. A., Hamilton, M. A. & Mole, D. R. (2019). U-Pb, trace element, and hafnium isotope composition of the Maniitsoq zircon? A potential new Archean reference material.

Goldschmidt Abstracts.

Mole, D. R., Barnes, S. J., Le Vaillant, M., Martin, L. A. J. & Hicks, J. (2018). Timing, geochemistry and tectonic setting of Ni-Cu sulfide-associated intrusions of the Halls Creek Orogen, Western Australia. *Lithos* **314–315**, 425–446.

Münker, C., Weyer, S., Scherer, E. & Mezger, K. (2001). Separation of high field strength elements (Nb, Ta, Zr, Hf) and Lu from rock samples for MC-ICPMS measurements. *Geochemistry, Geophysics, Geosystems* **2**, paper number 2001GC000183.

Patchett, P. J. & Tatsumoto, M. (1981). A routine high-precision method for Lu-Hf isotope geochemistry and chronology. *Contributions to Mineralogy and Petrology* **75**, 263–267.

Paton, C., Hellstrom, J., Paul, B., Woodhead, J. & Hergt, J. (2011). Iolite: Freeware for the visualisation and processing of mass spectrometric data. *Journal of Analytical Atomic Spectrometry* **26**, 2508–2518.

Pin, C. & Zalduegui, J. F. S. (1997). Sequential separation of light rare-earth elements, thorium and uranium by miniaturized extraction chromatography: Application to isotopic analyses of silicate rocks. *Analytica Chimica Acta* **339**, 79–89.

Powell, R. & Holland, T. J. B. (1988). An internally consistent dataset with uncertainties and correlations: 3. Applications to geobarometry, worked examples and a computer program. *Journal of Metamorphic Geology* **6**, 173–204.

Ravenelle, J. F., Weiershauser, L. & Cole, G. (2017). *Updated Independent Technical Report for the Maniitsoq Nickel-Copper-Cobalt-PGM Project, Greenland*. Toronto.

Savard, D., Barnes, S. J. & Meisel, T. (2010). Comparison between nickel-sulfur fire assay Te co-precipitation and isotope dilution with high-pressure asher acid digestion for the determination of platinum-group elements, rhenium and gold. *Geostandards and Geoanalytical Research* **34**, 281–291.

Scherer, E. E., Cameron, K. L. & Blichert-Toft, J. (2000). Lu-Hf garnet geochronology: Closure temperature relative to the Sm-Nd system and the effects of trace mineral inclusions. *Geochimica et Cosmochimica Acta* **64**, 3413–3432.

Sláma, J. *et al.* (2008). Plešovice zircon - A new natural reference material for U-Pb and Hf isotopic microanalysis. *Chemical Geology* **249**, 1–35.

Stacey, J. S. & Kramers, J. D. (1975). Approximation of terrestrial lead isotope evolution by a two-stage model. *Earth and Planetary Science Letters* **26**, 207–221.

Steiger, R. H. & Jäger, E. (1977). Submission on geochronology: Convention on the use of decay constants in geo- and cosmochronology. *Earth and Planetary Science Letters* **36**, 359–362.

Stern, R. A., Bodorkos, S., Kamo, S. L., Hickman, A. H. & Corfu, F. (2009). Measurement of SIMS instrumental mass fractionation of Pb isotopes during zircon dating. *Geostandards and Geoanalytical Research* **33**, 145–168.

Tanaka, T. *et al.* (2000). JNdi-1: A neodymium isotopic reference in consistency with LaJolla neodymium. *Chemical Geology* **168**, 279–281.

Tedeschi, M. T., Hagemann, S. G., Kemp, A. I. S., Kirkland, C. L. & Ireland, T. R. (2020). Geochronological constrains on the timing of magmatism, deformation and mineralization at the Karouni orogenic gold deposit: Guyana, South America. *Precambrian Research* **337**, 105329.

Waterton, P., Pearson, D. G., Mertzman, S., Mertzman, K. & Kjarsgaard, B. A. (2020). A fractional crystallisation link between komatiites, basalts, and dunites of the Palaeoproterozoic Winnipegosis Komatiite Belt, Manitoba, Canada. *Journal of Petrology*.

Weyer, S., Münker, C., Rehkämper, M. & Mezger, K. (2002). Determination of ultra-low Nb, Ta, Zr and Hf concentrations and the chondritic Zr/Hf and Nb/Ta ratios by isotope dilution analyses with multiple collector ICP-MS. *Chemical Geology* **187**, 295–313.

White, R. W., Powell, R., Holland, T. J. B., Johnson, T. E. & Green, E. C. R. (2014). New mineral activity–composition relations for thermodynamic calculations in metapelitic systems. *Journal of Metamorphic Geology* **32**, 261–286.

White, R. W., Powell, R., Holland, T. J. B. & Worley, B. A. (2000). The effect of TiO2 and Fe2O3 on metapelitic assemblages at greenschist and amphibolite facies conditions: mineral equilibria calculations in the system K2O–FeO–MgO–Al2O3–SiO2–H2O–TiO2–Fe2O3. *Journal of Metamorphic Geology* **18**, 497–511.

Wiedenbeck, M., Alle, P., Corfu, F., Griffin, W. L., Meier, M., Oberli, F., Von Quadt, A., Roddick, J. C. & Spiegel, W. (1995). Three natural zircon standards for U-Th-Pb, Lu-Hf, trace element and REE analyses. *Geostandards Newsletter* **19**, 1–23.